https://doi.org/10.31436/iiumej.v26i3.3497

DYNAMIC ANALYSIS ON AN AERIAL WORK PLATFORM USING A HYBRID CAD APPROACH FOR SATELLITE TESTING APPLICATIONS

NOR MOHD HAZIQ NORSAHPERI [1], SALMIAH AHMAD[2*], SITI FAUZIAH TOHA[3], MOHD AZRI ABD MUTALIB[4], MOHAMAD RIDZWAN ISHAK[5], DONG EUI CHANG[5]

[1]Department of Electrical and Electronics Engineering, Faculty of Engineering, Universiti Putra Malaysia, 43000, UPM Serdang, Selangor, Malaysia
[2]College of Engineering and Technology, University of Doha for Science and Technology, Doha, 24449, Qatar
[3]Department of Mechatronics Engineering, Kulliyyah of Engineering, International Islamic University Malaysia, 50728, Kuala Lumpur, Malaysia
[4]Machine Design Section, Machinery Technology Centre, SIRIM Berhad, 44200, Hulu Selangor, Selangor, Malaysia
[5]Department of Aerospace Engineering, Faculty of Engineering, Universiti Putra Malaysia, 43000, UPM Serdang, Selangor, Malaysia
[6]School of Electrical Engineering, Korea Advanced Institute of Science and Technology, Daejeon, Republic of Korea

**Corresponding author: salmiah.ahmad@udst.edu.qa*

(Received: 11 December 2024; Accepted: 22 March 2025; Published online: 9 September 2025)

ABSTRACT: This paper presents a dynamic analysis using a hybrid CAD model approach, focusing on a motorized adjustable vertical platform's lifting and baseplate loading subsystems as a case study. The hybrid CAD model approach allows for examining mechanism behaviours such as acceleration torque, speed variation, and jerk rates, as well as their impact on the total torque required by the subsystems. The analysis starts by developing 3D and 2D models with velocity profiles, followed by comprehensive analyses. The most interesting part of the study is that while the acceleration torque rate is high, its influence is minimal due to small accelerations and decelerations at approximately -5×10^{-5} m/s^3 to 3.1×10^{-5} m/s^3 within the subsystem. Additionally, torque requirements for the lifting subsystem remain consistent at 631.22 N·m at the highest position and 364.16 N·m at the lowest position across different speed modes. The study also evaluates jerk rates during acceleration and deceleration to ensure compliance with ISO standards for ride quality. This approach shows promise for developing heavy-duty autonomous aerial work platforms, especially in the space industry, where understanding system behaviours is crucial before the development process begins.

ABSTRAK: Kajian ini membentangkan analisis dinamik menggunakan pendekatan model hibrid CAD, dengan tumpuan kepada subsistem pengangkatan dan pemuatan plat asas (baseplate loading subsystem) bagi platfom menegak boleh laras bermotor (motorised adjustable vertical platform) sebagai kajian kes. Pendekatan model hibrid CAD ini membolehkan pemerhatian terhadap tingkah laku mekanisme seperti kadar tork pecutan, variasi kelajuan, dan kadar kejutan, serta impaknya terhadap jumlah tork yang diperlukan oleh subsistem. Analisis dimulakan dengan pembangunan model 3D dan 2D dengan profil kelajuan, diikuti dengan analisis komprehensif. Penemuan paling menarik yang didapati pada kajian ini adalah walaupun kadar tork pecutan tinggi, pengaruhnya sangat minimum kerana pecutan dan penghentian kecil dalam subsistem iaitu sekitar -5 x 10-5 m/s3 hingga 3.1 x 10-5 m/s3. Tambahan, keperluan tork bagi mengangkat subsistem kekal konsisten pada 631.22 N.m pada posisi tertinggi dan posisi terendah pada 364.16 N.m merentasi pelbagai mod

https://doi.org/10.31436/iiumej.v26i3.3497

kelajuan. Kajian ini juga menilai kadar kejutan semasa pecutan dan pengurangan kelajuan bagi memastikan pematuhan piawaian ISO bagi kualiti tunggangan. Pendekatan ini menunjukkan potensi dalam membangunkan platform kerja berat di udara secara autonomi, terutama dalam industri angkasa, di mana pemahaman tingkah laku sistem adalah penting sebelum proses pembangunan bermula.

KEYWORDS: *Dynamic Analysis, Scissor Mechanism, Satellite Test, and CAD Modelling*

1. INTRODUCTION

The thermal and vacuum test is one of the significant satellite tests that can be performed using a Thermal Vacuum Chamber (TVC), located in a clean room, as illustrated in Figure 1. To avoid any malfunction of the components in the satellite before the tests, as various components and the satellite itself are very sensitive to external particles, the cleanliness of the environment and specifications of the clean room are very important and shall be preserved [1, 2]. Commonly, the available facility for unloading and loading is the overhead crane, which poses a risk to the safety of the satellite and the operators because such a crane is sensitive to external force disturbances and hence, prone to oscillate [1, 3–5]. These limitations of the overhead crane significantly impact the operation and satellite safety, as the clean room is a confined space. Besides, the overhead crane is incongruous when loading and unloading, particularly when transferring the load inside the TVC. This is because the overhead crane does not have telescopic or horizontal motion, requires the travel system or rails to move, and has a limited working area. Hence, a customised adjustable vertical platform (MAVeP) is introduced to overcome the limitations of the overhead crane.

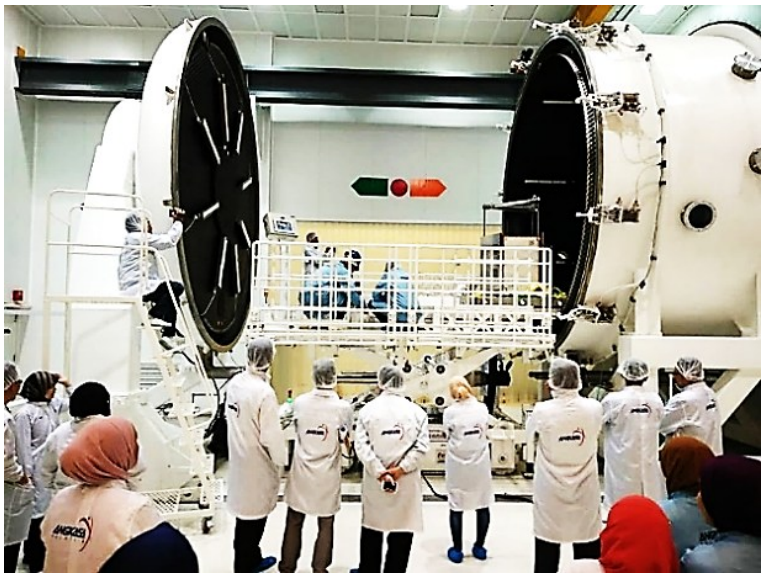

Figure 1. Thermal vacuum chamber overview.

Various analyses have been done to assess the mechanical forces acting on the actuator of an aerial work platform, such as the studies in [6–8] where most of these studies were carried out by conducting static analysis using the structural analysis method. Many other researchers have analysed the structure of the hydraulic actuator instead of the electrical-type actuator. For example, there is research on structural rigidity in [9], structure stiffness in [10], ground impact force in [11], platform stability in [12, 13] and hydraulic actuators in [14–17]. However, the only mechanical analysis done on the actuator is the static analysis using the structural analysis method. Not much research has been conducted on the dynamic analysis of the actuator, especially for the electrical-type actuator, compared to the hydraulic.

https://doi.org/10.31436/iiumej.v26i3.3497

Several attempts have been made to conduct static and dynamic analyses of structures. The study in [18] proposes a higher-order strain-based element to enhance the accuracy of finite element analysis for plane structures by using higher-order polynomials to represent the deformation field. The strain-based approach has also been adopted in [19] to analyse the behaviour of materials near cracked structures. Other than the strain-based methods, the study in [20] introduces a dynamic model to analyse the behaviour of the aerial work platform during horizontal motion by considering mass distribution, external forces, and the system's dynamic response. Furthermore, the dynamic analysis was also conducted in [21] to evaluate the behaviour of the lifting arm system by developing the dynamic model of the system using the Lagrange equation. However, a significant problem with the aforementioned numerical approaches to studying the behaviour of a complex system is that they are challenging and prone to error.

Recent studies in [22–25] have suggested that computer-aided design (CAD) is becoming essential in analysing the dynamic behaviours of complex mechanical systems in modern engineering tools. In [26], the CAD model is adopted to enhance the accuracy of the reverse engineering process. The study in [27] also shows the importance of CAD techniques in obtaining a detailed and accurate model representing historical machinery. This allows for in-depth analysis of the equipment's design, construction, and functioning, providing insights into technological advancements and engineering practices. Other than the studies above, the CAD model has also been utilised to generate the robot path trajectories by using the mesh, as discussed in [28]. Despite ongoing efforts, it remains a continual challenge to work with highly complex surfaces using CAD techniques [29]. Moreover, there has been minimal discussion on the mechanical forces acting on the electrical actuators of an aerial work platform.

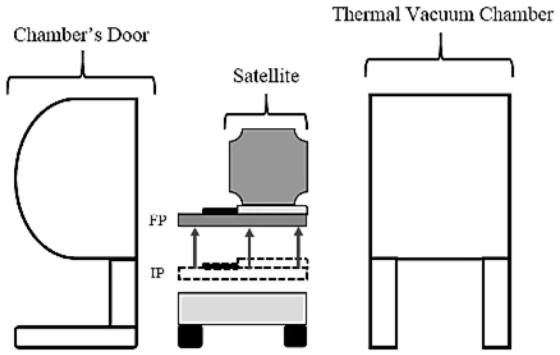

*FP: Final Position, IP: Initial Position

(a) Lifting Subsytem

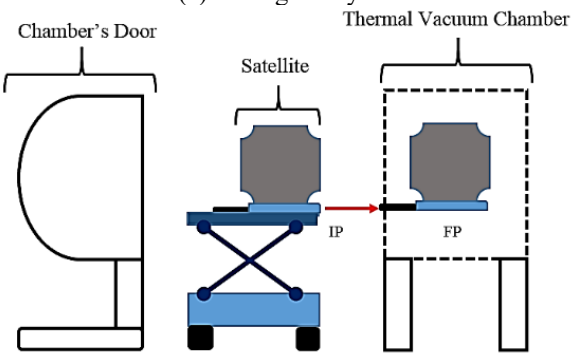

*FP: Final Position, IP: Initial Position

(b) Baseplate Loading Subsystem

Figure 2. Vertical and horizontal positioning mechanisms

https://doi.org/10.31436/iiumej.v26i3.3497

Considering all, the primary aim of this paper is to conduct the dynamic analysis of the lifting and baseplate loading subsystems in MAVeP that can perform horizontal and vertical movements, as described in Figure 2 using the hybrid CAD model approach and considering the findings in [24]. The proposed hybrid CAD model approach utilizes both 3D and 2D models of MAVeP to conduct the dynamic analysis, as it has been reported that virtual models are one of the most practical tools for assisting practitioners in decision-making [29]. Additionally, this study aims to create a CAD model that closely resembles MAVeP, enabling a comprehensive illustration of the engineering significance of the invention and facilitating a deeper understanding of its functionality. To the best of the authors' knowledge, this study represents one of the earliest developments of an autonomous mobile aerial platform for satellite test facilities and clean room operations. Therefore, this study contributes significantly to research on dynamic analysis using the proposed hybrid CAD model approach and to the field of autonomous aerial work platforms for satellite test facilities.

Note that MAVeP is actuated by electric motors and functions within clean rooms or confined spaces as an additional satellite handling platform, particularly suited for thermal and vacuum testing. Moreover, the lifting and baseplate loading subsystems denote the mechanisms that provide vertical and horizontal motions, respectively. Several crucial analyses are required before selecting the electrical motor specifications and fabrication processes for MAVeP. These include designing the velocity profile, conducting acceleration and jerk analyses, and torque analysis for both the lifting and baseplate loading subsystems, using the actual specifications of MAVeP. The overall process to analyse the dynamic behaviour of the lifting and baseplate loading subsystems is shown in Figure 3.

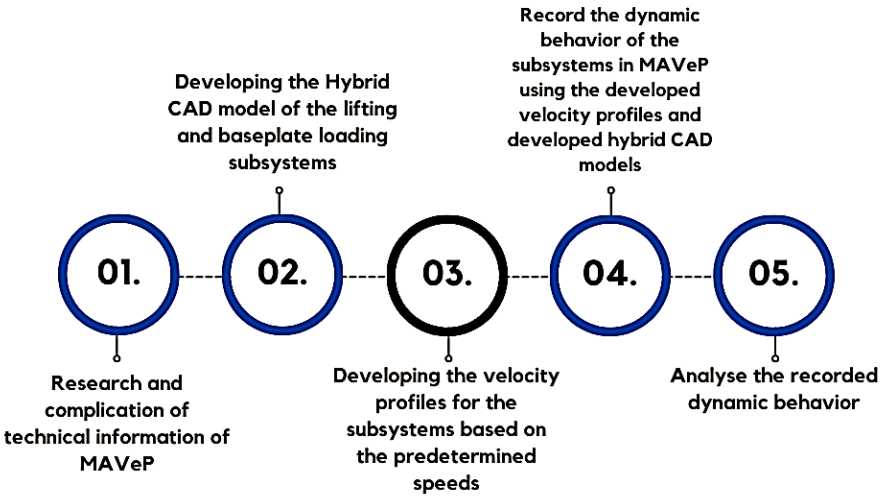

Figure 3**.** Flowchart of the dynamic analysis.

This paper is organized as follows: Section 2 describes the subsystem mechanisms and their properties, followed by Section 3, which explains the velocity profile design based on the prescribed subsystem speeds. The final two sections, 4 and 5, summarize the main findings of this study and present the conclusion, respectively.

2. HYBRID CAD MODELS

This section describes the mechanisms in MAVeP responsible for translating horizontal and vertical motions, referred to as the baseplate loading and lifting subsystems, respectively, along with their structural properties. The lifting subsystem utilizes a scissor mechanism, ball screw, and electrical motor, while the baseplate loading subsystem integrates a rack and pinion

https://doi.org/10.31436/iiumej.v26i3.3497

mechanism with an electrical motor. Then, this section explains the proposed hybrid CAD models of both subsystems for the dynamic analysis.

2.1. Vertical motion mechanism for lifting subsystem

The overall structural design of the MAVeP was designed, as shown in Figure 4, in the SOLIDWORKS 3D environment for the motion study and dynamic analysis. The structure consists of a multiple-link combination as depicted in Figure 5. At the stowed position, the minimum height of the platform is estimated to be 0.79 m, and the highest position the platform can reach is 1.48 m. The electrical motor was decided to be used for the mechanism, and the servomotor was selected. The servomotor for lifting the subsystem ($M1$) is fixed with a clamper ($C1$), as shown in Figure 5. The motor provides rotational motion, and the motion is converted into linear motion by a ball screw (BS) where the ball screw is mounted using a clamper ($C2$). Each clamper moves in linear motion and is attached with four links ($SS1$, $SS2$, $SS3$ and $SS4$). The end of each link ($SS1$, $SS2$, $SS3$ and $SS4$) is attached to the four main scissors (MS). If the power is fed to the motor, the motor shaft will rotate along with the ball screw, where the rotational motion is converted into linear motion, as in Figure 6. When the clampers ($C1$ and $C2$) is moving, each link ($SS1$, $SS2$, $SS3$ and $SS4$) rotates with respect to the rotational point on each clamper.

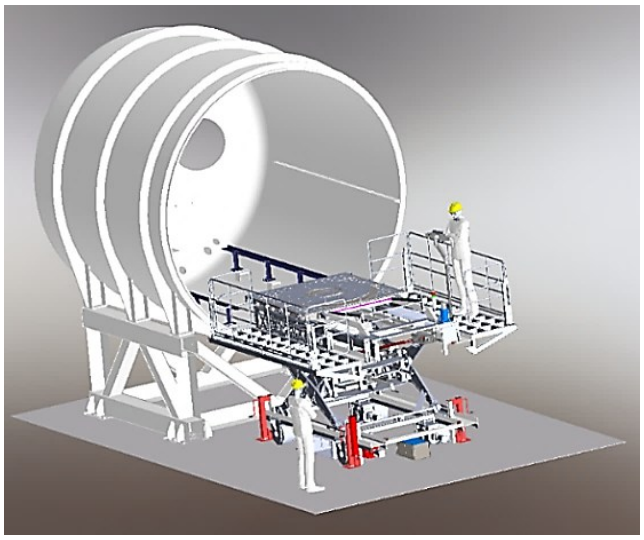

Figure 4. The MAVeP design in the SOLIDWORKS software.

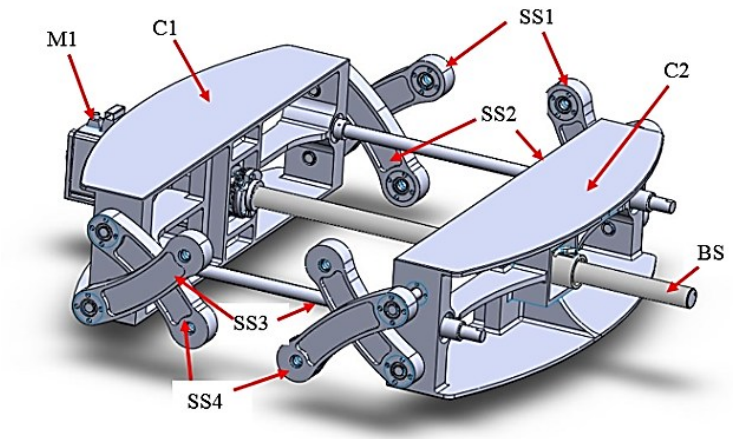

Figure 5. Clamper structure with the motor and ball Screw.

https://doi.org/10.31436/iiumej.v26i3.3497

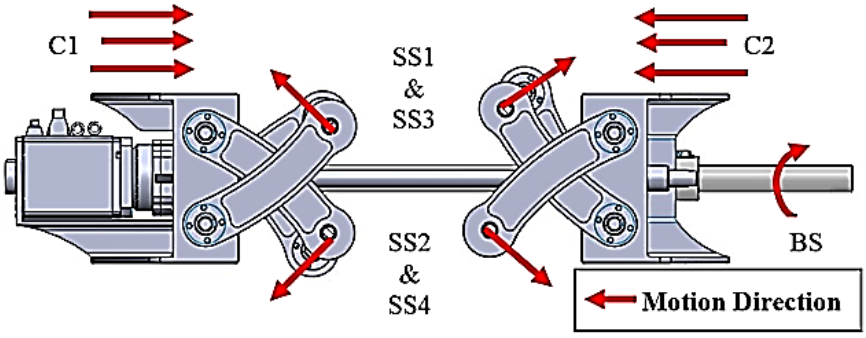

Figure 6. Clamper motion when the platform height is increasing.

Figure 7 illustrates the overall motion of the lifting subsystem. When the main scissors rotate with respect to the link's angular position, θ_{ms}, the height of the upper platform (UP) changes, as shown in Figure 6. Based on Figure 6, the height changes due to the joints on the platform, where the main scissors (MS) are rotating at the hinge joint on the upper platform (UP) and the base platform (BP). During the platform height change, the end of each main scissor slides on the slider, located at both UP and BP.

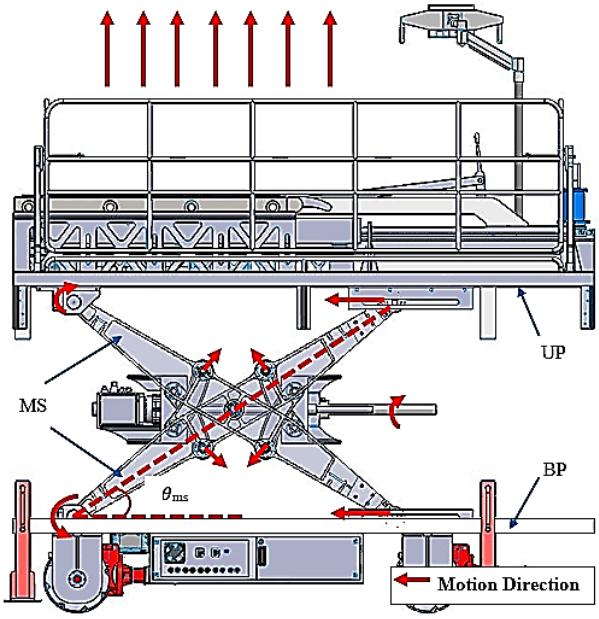

Figure 7. Lifting subsystem working principle.

Figure 8 illustrates that the lifting subsystem consists of similar motions on both the right and left sides of the platform. If the system is configured using a 3D model as depicted in Figure 8, a redundancy issue exists, which may lead to high computational efforts and inaccurate dynamic analysis. To simplify and avoid redundancy, the study utilised the 2D model technique, shown in Figure 9 was used to consider that both sides have similar motions and configurations. Note that all parts were designed based on structural characteristics, and mass properties were assigned before starting the analysis, based on Table 1. Testing revealed no redundancy in the 2D model compared to the 3D model, which had over 10 redundancies.

https://doi.org/10.31436/iiumej.v26i3.3497

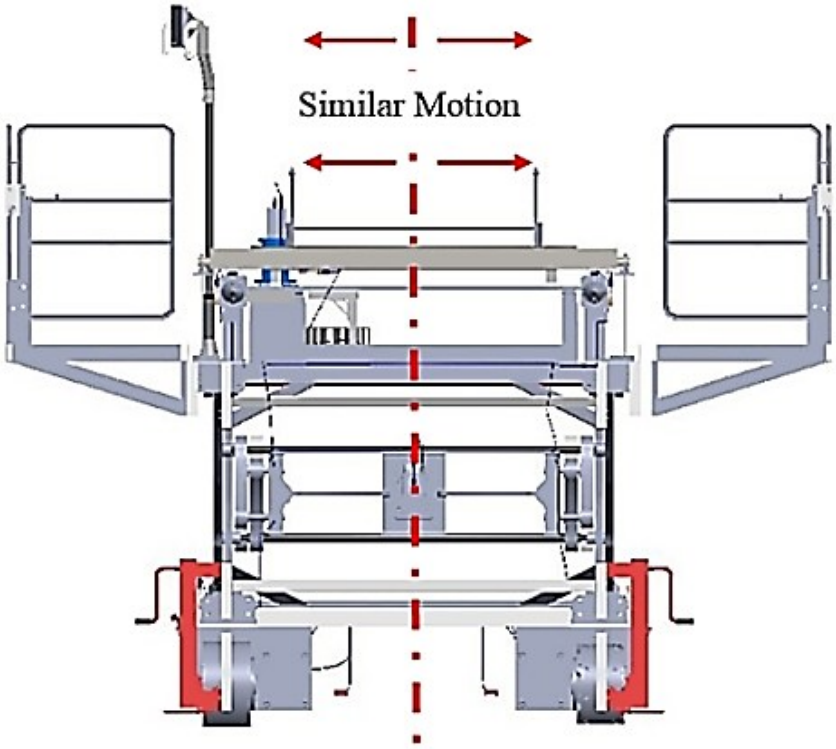

Figure 8. Similar mates and motions.

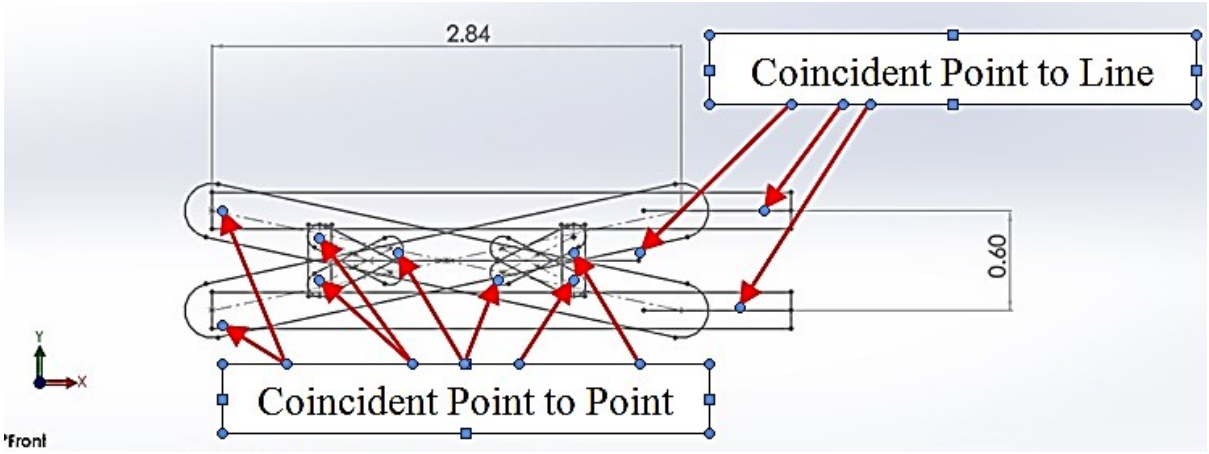

Figure 9. Lifting subsystem 2D model.

Table 1. MAVeP mechanical properties

No.	Structure	Properties
1	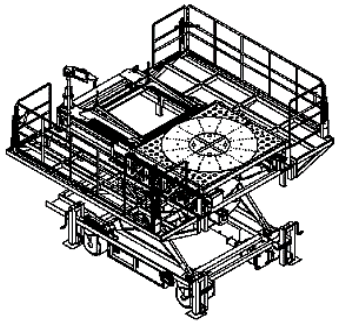	Name: All structures Estimated Weight: 7538.5 kg Satellite Weight: 1500 kg Operators' Weight: 200 kg Upper Deck Weight (UP): 1368.5 kg Lower Deck Weight (BP): 2830 kg

https://doi.org/10.31436/iiumej.v26i3.3497

No.	Structure	Properties
2	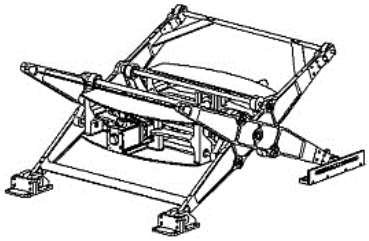	Name: Lifting Mechanism Estimated Weight: 1840 kg
3	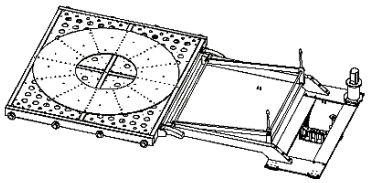	Name: Baseplate Loading Estimated Weight: 1000 kg Baseplate Dimension: 1.94 x 1.64 x 1.00 m
4		Name: Main Scissor Estimated Weight: 92.06 kg Length: 2.9 m Notation: MS
5	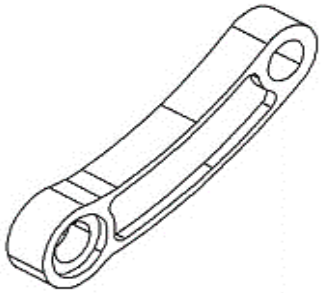	Name: Small Scissor Estimated Weight: 37.0 kg Length: 3.85 m Notation: $SS1$, $SS2$, $SS3$ and $SS4$
6	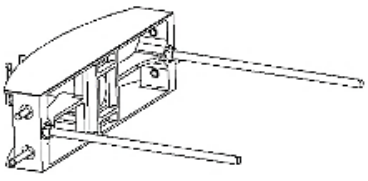	Name: Clamper Estimated Weight: 640 kg Dimension: 1.39 x 0.54 x 0.41 m Notation: $C1$
7	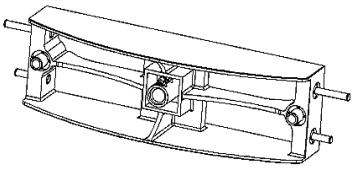	Name: Ball Screw Clamper Estimated Weight: 347 kg Dimension: 1.39 x 0.54 x 0.41 m Notation: $C2$

https://doi.org/10.31436/iiumej.v26i3.3497

2.2. Horizontal motion for baseplate loading subsystem

The baseplate loading subsystem utilises the rack and pinion (RP) mechanism along with the servomotor, as depicted in Figure 10 and 11. Figure 10 provides detailed insight into the working principle of the baseplate loading subsystem. Based on Figure 10, the subsystem is positioned on the upper platform (UP), where the satellite undergoes thermal testing while placed on the baseplate. A clamp ($C3$) secures the baseplate to the mechanism housing the rack and pinion. The baseplate can travel a maximum distance of 3.0 m from its initial position. As shown in Figure 11, this subsystem is straightforward, with the motor ($M2$) directly connected to the pinion, generating rotational motion that is then converted into linear motion of the rack. The combination of the motor and the pinion produces the rotational motion and is converted into the linear motion of the rack.

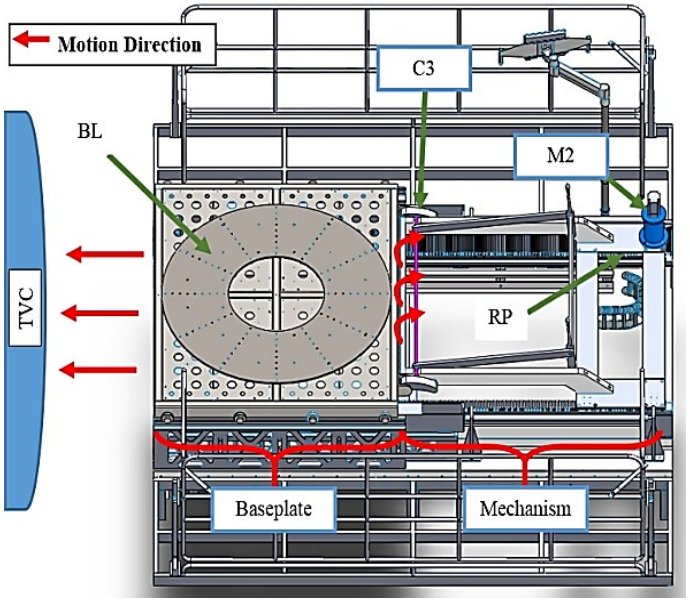

Figure 10. The baseplate loading subsystem configuration (top view).

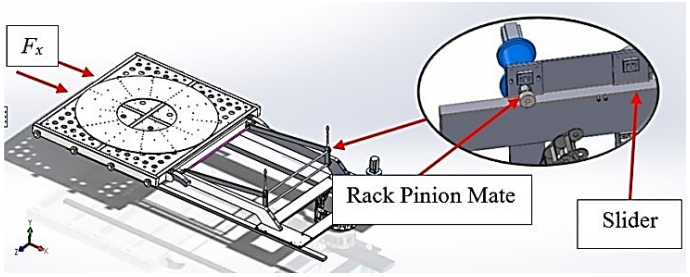

Figure 11. Baseplate loading subsystem 3D model.

Table 2. Selected mechanical attachments

No.	Item	Properties
1	Rack and Pinion	Guide Friction Coefficient: 0.03 Maximum Load: 1280 N Number of Teeth: 20 Pinion Pitch: 0.0637 m
2	Ball Screw	Lead: 0.016 m Maximum Load: 178.9 kN Nut Mass: 17.4 kg Shaft Mass: 40.4 kg

https://doi.org/10.31436/iiumej.v26i3.3497

The 3D model technique was employed for the baseplate loading subsystem due to its simplicity. This method facilitated the implementation of additional mating configurations using mechanical mates in SOLIDWORKS, enabling the system to be set up effectively. Mechanical mates offer various options, including cam, slot, gear, hinge, screw, and rack-and-pinion mates. Hence, the rack and pinion properties listed in Table 2 were incorporated into the motion study. The overall configuration is depicted in Figure 11, and no motion redundancy was found.

3. VELOCITY PROFILE DESIGN

Before analysing the dynamic behaviour of MAVeP, it is essential to elucidate the velocity profile designs utilized for MAVeP operation and dynamic analysis. The researchers detail the speed requirements for each MAVeP subsystem in [1]. For the MAVeP operation, a low velocity is preferred as the operators will be on the platform during the process (loading and unloading). During MAVeP operation, a preference is given to low velocity, as operators will be on the platform during the satellite testing. High velocity can result in sudden movements (jerk), posing safety risks. To mitigate these risks, a velocity profile is employed to regulate acceleration and prevent sudden movements, as detailed in [30, 31], thereby reducing forces exerted around the motor and minimizing motor torque. This velocity profile aims to ensure smooth, fast, and precise motion, avoiding jerking at the start or stop of MAVeP movement, as discussed in [12, 32]. A commonly used approach for designing the velocity profile is the trapezoidal profile, as outlined in [31, 33]. Power consumption can be reduced by segmenting the total operating time into thirds, given that power is inversely proportional to time. Minimizing angular acceleration, a in Eqs. (1)–(3) can reduce the torque and power the servomotor requires. Figure 12 shows a typical velocity profile.

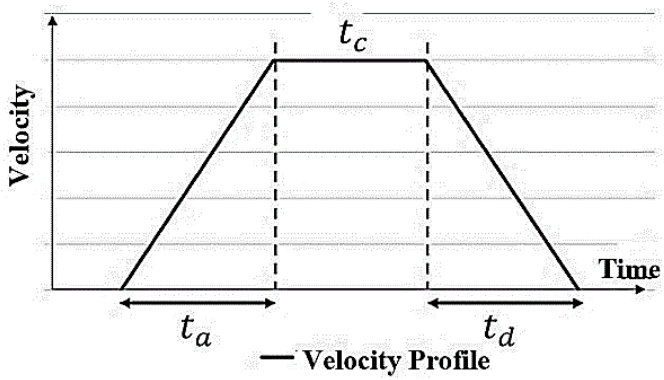

Figure 12. General trapezoidal velocity profile.

First, the motor torque, T_M can be defined as

$$T_M = SF(T_T) \tag{1}$$

$$T_T = T_a + T_L + T_d \tag{2}$$

$$T_a = J_T a \tag{3}$$

where, T_T, T_a, T_L, T_d, J_T and SF denote the total torque, acceleration torque, constant velocity torque, deceleration torque, system moment of inertia, and safety factor, respectively. The general formulae for designing the velocity profile can be described in Eq. (4):

$$D_{Total}(t) = D_a(t) + D_c(t) + D_d(t) \tag{4}$$

https://doi.org/10.31436/iiumej.v26i3.3497

where D_{Total} is the total distance, D_a is the acceleration distance, D_c is the constant velocity distance and D_d is the deceleration distance in the time domain, t. The total distance can be expanded as in Eqs. (5)-(6):

$$D_{Total}(t) = \frac{V_{max}(t)(T_a)}{2} + V_{max}(t)(T - t_a - t_d) + \frac{V_{max}(t)(t_d)}{2} \tag{5}$$

$$D_{Total}(t) = V_{max}(t)(T) - V_{max}(t)(t)\left(\frac{t_a + t_d}{2}\right) \tag{6}$$

where, $V_{max}(t), T, t_a, t_d$ and t_c represent the maximum velocity, total required time, acceleration time, deceleration time, and constant velocity-time, respectively. Then Eq. (6) is rearranged to obtain Eq. (7).

$$V_{max}(t) = \frac{D_{Total}(t)}{T - \frac{t_a + t_d}{2}} \tag{7}$$

t_a and t_d can be defined as shown in Eq. (8). When substituted into Eq. (7), this can be simplified as in Eq. (9), enabling the determination of the total travel time, T in terms of the total travel distance, $D_{Total}(t)$ and maximum velocity, $V_{max}(t)$.

$$\mathrm{t_a = t_d = t_c = \frac{1}{3}T} \tag{8}$$

$$\mathrm{T = \frac{3D_{Total}(t)}{2V_{max}(t)}} \tag{9}$$

The total travel time, T can be computed by substituting the total distance, $D_{Total}(t)$ and maximum velocity, $V_{max}(t)$ in Eq. (9). As T is obtained, the values of t_a, t_d and t_c can be known by solving Eq. (8) to design the velocity profile, as shown in Figure 12. This section has focused on the preliminary design of the velocity profile. The following subsections describe the velocity profile for each subsystem.

3.2. Velocity profile for lifting subsystem

The lifting subsystem has two-speed modes called high and low-speed modes, as stated in [1]. The velocity of the clamper, C1 has been first determined to produce the prescribed speed of the upper platform, UP and the velocity of the clamper is recorded as tabulated in Table 3. To analyse the lifting subsystem's dynamic behaviour, the velocity profiles for the servomotors of the lifting subsystem, as shown in Figure 13, are then developed. These profiles, generated to achieve the prescribed speed of the clamper, C1 in Table 3, are applied to the lifting subsystem in both high and low-speed modes.

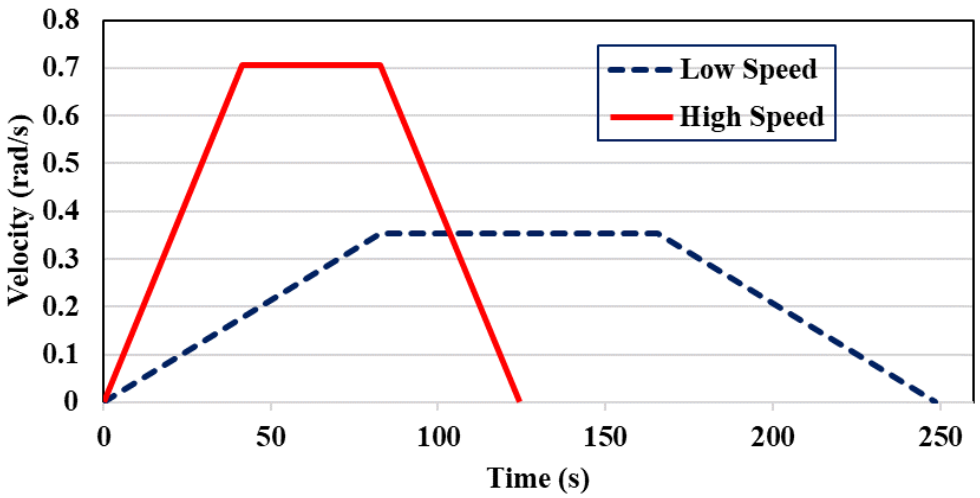

Figure 13. The velocity profiles for the servomotor of the lifting subsystem.

https://doi.org/10.31436/iiumej.v26i3.3497

Table 3. Speed requirements for the lifting subsystem

Speed (m/s)	$C1$	UP
High	0.0018	0.0083
Low	0.0009	0.0042

3.2. Velocity profile for baseplate loading subsystem

For the baseplate loading subsystem, a velocity profile was developed explicitly for the servomotor, $M2$, as in Figure 10, to achieve the predetermined speed of the baseplate mechanism (RA), as documented in [1] and detailed in Table 4. The baseplate of MAVeP should move with only one speed, which is 0.0042 m/s. To achieve the speed of the baseplate servomotor, $M2$, should operate at 0.1386 rad/s. Hence, the velocity profile in Figure 14 was generated based on this servomotor speed for the dynamic analysis.

Table 4. Speed assigned for the baseplate loading subsystem

	Servomotor ($M2$)	Baseplate Mechanism (RA)
Speed	0.1386 rad/s	0.0042 m/s

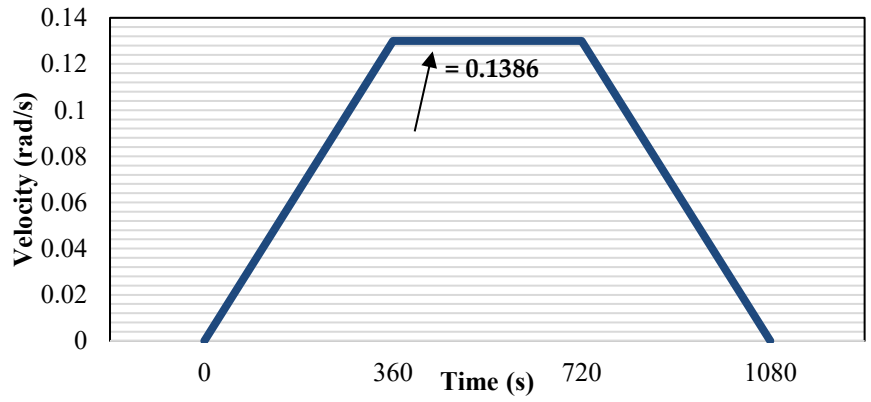

Figure 14. The baseplate loading motor, M2 velocity profile.

4. RESULTS AND DISCUSSION OF DYNAMIC ANALYSIS OF THE SUBSYSTEMS

Section 3 comprehensively describes the velocity profile designs for each subsystem in MAVeP. In this section, the dynamic behaviors of each subsystem under the designed velocity profiles shown in Figure 15 and Figure 14, for the lifting (in Figure 9) and baseplate loading (in Figure 11) subsystems, respectively, are analysed. The study was done based on the actual structure specifications, as described in Section 2. This section discusses the dynamic behaviours of the subsystems, such as the acceleration torque, jerk, and velocity.

4.1. Acceleration and jerk analysis

When determining servomotor specifications, the acceleration torque plays a crucial role as it can affect the total torque required by the system. Figure 16 shows the computed acceleration of the designed velocity profiles for the lifting subsystem. Based on the figure, the accelerations are $\pm 4.347 \times 10^{-5}$ m/s^2 for the high speed and $\pm 1.08 \times 10^{-4}$ m/s^2 for the low speed. By referring to Eq. (2), the acceleration torque influences the total torque. However, in this study, the acceleration torque can be disregarded in total torque measurement due to the small acceleration and deceleration of the lifting subsystem (approximately between 10^{-4} m/s^2 and

https://doi.org/10.31436/iiumej.v26i3.3497

10^{-5} m/s^2). Furthermore, the maximum jerk, representing a quick or sudden movement, occurs during acceleration and deceleration at approximately 2.4 × 10^{-4} m/s^3 and 3.1 × 10^{-5} m/s^3 for the high and low speeds, respectively. This jerk rate falls within the low jerk category according to ISO 18738:2003, where the acceptable jerk rate for the elevator ride quality is approximately between 0 and 3.0 m/s^3 [34].

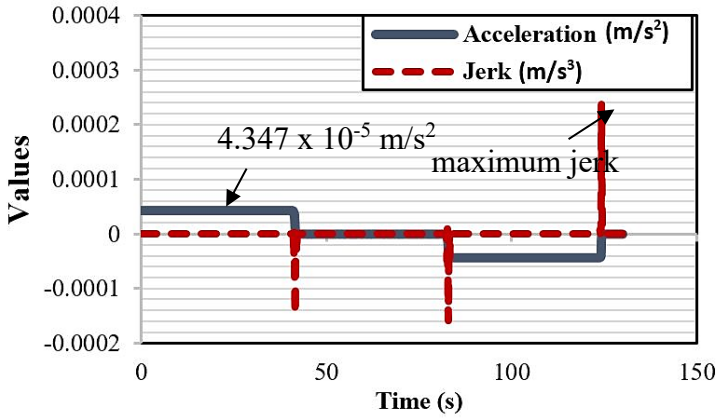

(a) High-speed mode

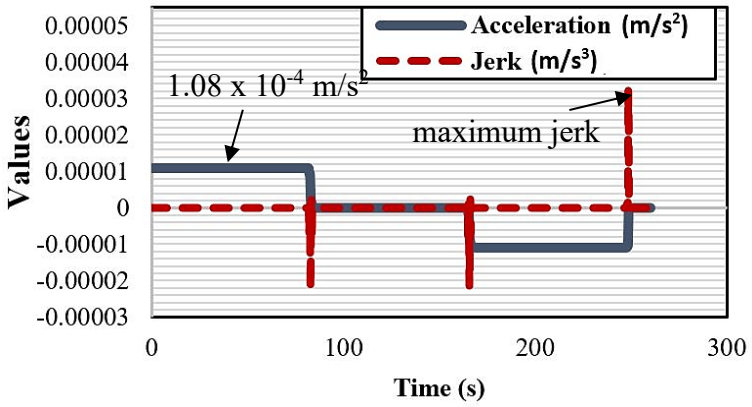

(b) Low-speed mode

Figure 16. Acceleration and jerk for the lifting subsystem

Figure 17 shows the acceleration and deceleration for the baseplate loading subsystem, both of which are ±1.15 × 10^{-5} m/s^2. The acceleration torque was disregarded because these values are minimal and comparable to those of the lifting subsystem. In this study, the maximum jerk observed was -5 × 10^{-5} m/s^3 at the end of the operation, which falls below the recommended jerk rate in the industry as documented in [34]. The overall findings for both subsystems in terms of acceleration and jerk can be summarised in Table 5. A minimum jerk rate is preferable, as a high jerk rate can lead to platform instability, which may significantly impact the safety of both the operator and any attached equipment, such as satellites. A lower jerk rate also helps reduce mechanical stress and fatigue on the mechanism, extending its operational lifespan.

Table 5. Acceleration and jerk of the subsystems

Subsystems	Lifting	Baseplate Loading
Standard Jerk [34]	0-3.0 m/s^3	0-5.0 m/s^3
High-speed Jerk	2.4 x 10^{-4} m/s^3	5 x 10^{-5} m/s^3
Low-speed Jerk	3.1 x 10^{-5} m/s^3	-
High-speed Acceleration	4.347 x 10^{-5} m/s^2	1.15 x 10^{-5} m/s^2
Low-speed Acceleration	1.08 x 10^{-4} m/s^2	-

https://doi.org/10.31436/iiumej.v26i3.3497

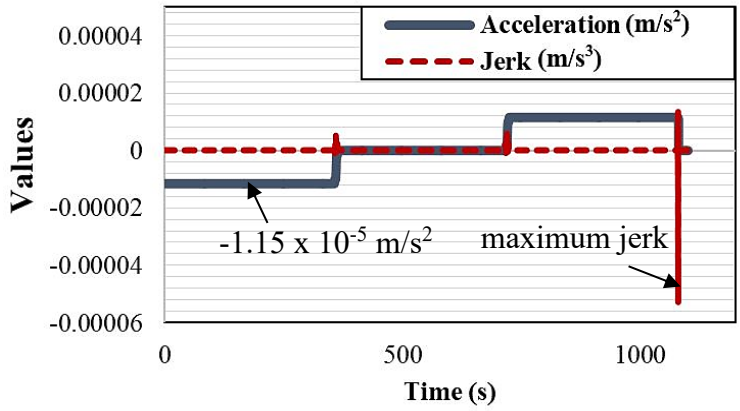

Figure 17. Acceleration and jerk for the baseplate loading subsystem.

4.2. Torque analysis for the subsystems

This study also examined the required torque. It determined the height position of the lifting subsystem and the speed mode (high or low speed) where the highest torque is required. Figure 18 shows the torques required for the servomotor of the lifting subsystem as it transitions from the stowed position to the highest position under the designed velocity profiles. As shown in Figure 18, it can be observed that the maximum torque required for both speeds is similar, which is 631.22 N.m at the highest position and 364.16 N.m at the lowest (stowed) position. The results of this study indicate that speed changes do not affect the maximum and minimum torque required for the servomotor of the lifting subsystem.

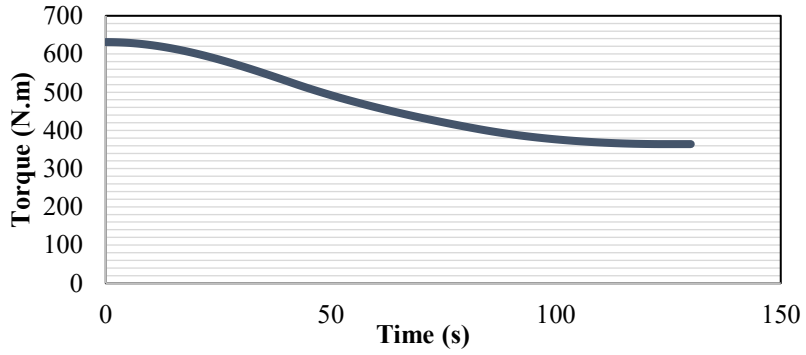

(a) High-speed Mode

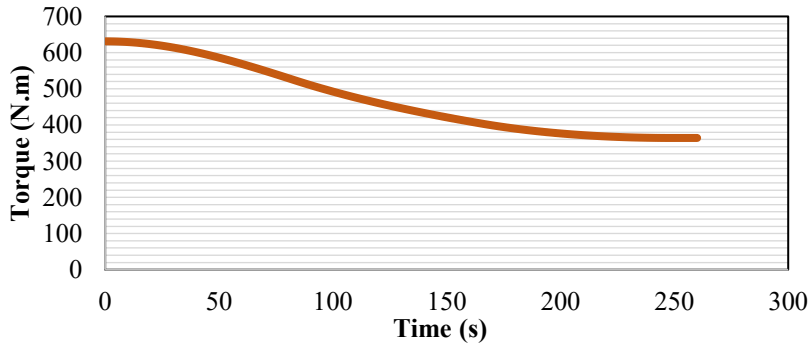

(b) Low-speed Mode

Figure 18. Servomotor torque requirements for the lifting subsystem

To further validate the results, the findings of this study are compared with those of the study in [24], where the numerical approach was used, as shown in Table 6. From Table 6, the

https://doi.org/10.31436/iiumej.v26i3.3497

result indicates that there is approximately a 28.38% difference. The motor torque was intentionally set higher for safety considerations in the actual system. This ensures that the servomotor does not operate at full power during operation, increasing flexibility and extending its lifespan. Referring to the study in [24], in practical application, the servomotor used for the lifting subsystem of actual MAVeP is 875 N.m, which is only approximately a 27.86% difference compared with the proposed CAD method. Despite a slight difference, the consistency between the proposed method and the real-world application indicates the reliability of our approach. This alignment strengthens confidence in the CAD method's accuracy and its potential for widespread adoption in similar engineering applications.

Table 6. Overview of torque analysis for the lifting subsystem

Speed Mode	**Proposed Method Torque Using 2D Model**	**Calculated Torque Using Numerical Analysis** [24]
Highest Torque (N.m)	631.22	491.69
Lowest Torque (N.m)	346.16	276.78

Figure 19 shows the torque requirements of the servomotor for the baseplate loading system, as determined through dynamic analysis with the proposed 3D CAD model. Based on Figure 19, the maximum torque is approximately 14.68 N.m, where the highest torque occurred during the acceleration, highlighting the significance of torque during this phase. Moreover, the findings show that the proposed velocity profile for the baseplate loading system offers a practical solution to minimize acceleration torque. By implementing this profile, engineers can reduce energy consumption and enhance the system's efficiency. Table 7 summarises the torques required for the baseplate loading subsystem. From the data in Table 7There is approximately only a 9.22% difference compared with the numerical analysis. However, the proposed CAD model provides a more practical and reliable approach compared to the cumbersome and error-prone nature of numerical analysis. This can help practitioners determine the required actuator torque without overspecification, thereby avoiding unnecessary weight and development costs without compromising performance.

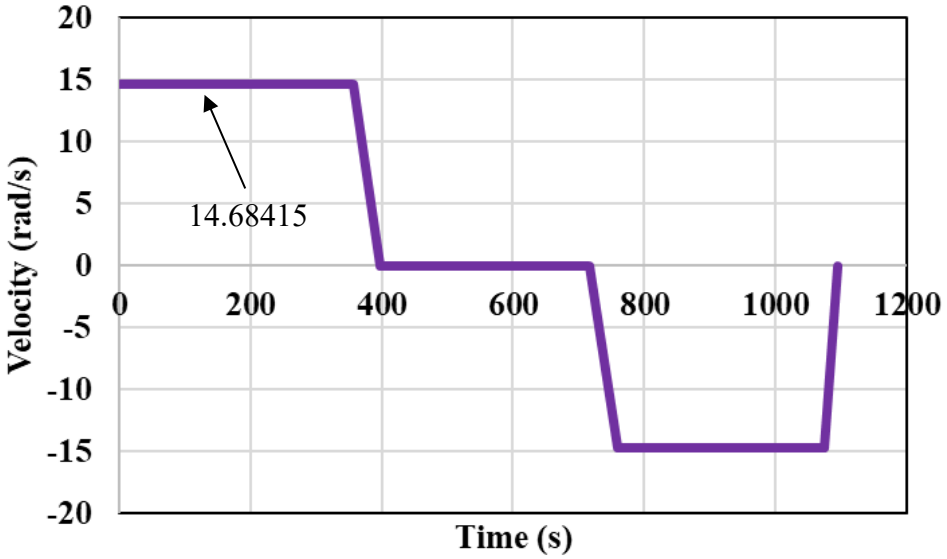

Figure 19. Servomotor torque requirements for the baseplate loading subsystem.

Table 7. Overview of torque analysis for the lifting subsystem

	Proposed Method Torque Using 3D Model	Calculated Torque Using Numerical Analysis
Torque (N.m)	14.68415	18.3793

5. Conclusion

In this study, the dynamic analysis of the lifting and baseplate loading subsystems using the hybrid CAD model was conducted, and the findings were discussed in detail. In summary, this study has shown that the hybrid CAD model, which consists of the 3D and 2D models, has helped practitioners study the dynamic behaviour of the lifting and baseplate loading subsystems of MAVeP without complex numerical formulation. This study also suggests the significance of considering acceleration torque when determining servomotor specifications for systems like the lifting subsystem. Despite the small accelerations and decelerations observed in this study, acceleration torque still impacts the total torque required by the system. Additionally, the study assesses the jerk rate during acceleration and deceleration, which is crucial for evaluating ride quality in systems like aerial work platforms. The observed jerk rates fall within acceptable limits according to ISO standards.

Other than that, the study identified the peak torque demands by determining the height position of the lifting subsystem and the speed mode (high or low speed). Interestingly, this finding suggests that speed changes do not significantly influence the torque demands of the lifting subsystem's servomotor. Such insights are crucial for optimizing servomotor specifications and ensuring efficient performance in practical applications. It is recommended that future research focus on further refining the proposed CAD model and exploring additional optimisation techniques to minimise torque requirements and improve overall system performance.

ACKNOWLEDGEMENT

This project was funded by the Ministry of Science, Technology and Innovation of Malaysia (MOSTI) through the Space Research Agency of Malaysia (ANGKASA) under the SP15-066-0188 grant. The Qatar National Library funded the publication of this article.

REFERENCES

[1] Leng EWL, Salleh N, Salim H, Sabri SF, Ismail M. (2015) Design and development of Motorized Adjustable Vertical Platform (MAVeP) for satellite test facility. In: 2015 Int. Conf. Sp. Sci. Commun. IEEE, pp 424–427.

[2] Norsahperi NMH, Ahmad S, Toha SF, Mutalib MAA. (2022) Design, Simulation and Experiment of PSO-FOPID Controller for Height Position Control of a Scissor. FME Trans, 50(1):46–54.

[3] Norsahperi NMH, Ahmad S, Toha SF, Mahmood IA, Hanif NHHM. (2018) Robustness analysis of fractional order PID for an electrical aerial platform. J Mech Sci Technol, 32(11):5411–5419.

[4] Lu B, Fang Y, Sun N. (2020) Adaptive Output-Feedback Control for Dual Overhead Crane System With Enhanced Anti-Swing Performance. IEEE Trans Control Syst Technol, 28(6):2235–2248.

[5] Chen H, Fang Y, Sun N. (2016) A Swing Constraint Guaranteed MPC Algorithm for Underactuated Overhead Cranes. IEEE/ASME Trans Mechatronics, 21(5):2543–2555.

[6] Spackman H. (1989) Mathematical Analysis of Scissor Lifts.

[7] Corrado A, Polini W, Canale L, Cavaliere C. (2016) To design a belt drive scissor lifting table. Int J Eng Technol, 8(1):515–525.

[8] Oliveira LFA de. (2018) Smart Materials Actuators : Actuated Scissor Lift. University of Porto.

[9] Lee-St.John A, Sidman J. (2013) Combinatorics and the rigidity of CAD systems. Comput Des, 45(2):473–482.

[10] Zhao D-J, Zhao J-S, Yan Z-F. (2016) Planar Deployable Linkage and Its Application in Overconstrained Lift Mechanism. J Mech Robot, 8(2):1–9.

[11] Pan CS, Chiou SS, Kau T-Y, Wimer BM, Ning X, Keane P. (2017) Evaluation of postural sway and impact forces during ingress and egress of scissor lifts at elevations. Appl Ergon, 65:152–162.

[12] Zhang W, Zhang C, Zhao J, Du C. (2015) A Study on the Static Stability of Scissor Lift. Open Mech Eng J, 9(1):954–960.

[13] Singh SK, Deepak SR. (2020) Analytical Reason for Smaller Lateral Sway in Angled-Plane Scissor Linkage. J Mech Robot, 12(5):1–9.

[14] Saxena A. (2016) Deriving a Generalized, Actuator Position-Independent Expression for the Force Output of a Scissor Lift. arXiv Prepr arXiv161110182, :1–18.

[15] Momin GG, Hatti R, Dalvi K, Bargi F, Devare R. (2015) Design, Manufacturing and Analysis of Hydraulic Scissor Lift. Int J Eng Res Gen Sci, 3(2):733–740.

[16] Qu FP, Xue Y. (2014) A High Precision and Convenient Method to Analyze the Mechanics of Scissor Lift Platform under the Action of Combined Loads. Appl Mech Mater, 618:503–508.

[17] Sun LB, Wang RR, Li XX. (2014) Lifting Force Calculation and Safty Analysis of Hydraulic Scissor Lift Platform. Adv Mater Res, 960–961:1450–1454.

[18] Rezaiee-Pajand M, Gharaei-Moghaddam N, Ramezani MR. (2019) A new higher-order strain-based plane element. Sci Iran, 26(4A):2258–2275.

[19] Rezaiee-Pajand M, Gharaei-Moghaddam N, Ramezani M. (2020) Strain-based plane element for fracture mechanics' problems. Theor Appl Fract Mech, 108(March):102569.

[20] Deng M, Ji A, Zhang L, Wang H, Zhao Z. (2022) Lateral vibration behaviors of the straight boom of the aerial work platform in the horizontal linear motion. Autom Constr, 134(December 2021):104095.

[21] Xiao W, Li C, Fan L, Li Q, Tan L. (2023) Dynamic Analysis of the Lifting Arm System in the Integrated Offshore Platform Decommissioning Equipment in Complicated Sea States. Processes. doi: 10.3390/pr11020645.

[22] Pappalardo CM, Del Giudice M, Oliva EB, Stieven L, Naddeo A. (2023) Computer-Aided Design, Multibody Dynamic Modeling, and Motion Control Analysis of a Quadcopter System for Delivery Applications. Machines, 11(4):464.

[23] Shabana AA. (2019) Integration of computer-aided design and analysis: application to multibody vehicle systems. Int J Veh Perform, 5(3):300.

[24] Norsahperi NMH, Ahmad S, Toha SF, Mahmood IA. (2021) Analysis and practical validation on a multi-linkage scissor platforms drive system for the satellite test facilities. Int J Heavy Veh Syst, 28(1):1.

[25] Kyratsis P, Kakoulis K, Markopoulos AP. (2020) Advances in CAD/CAM/CAE technologies. Machines, 8(1):13.

[26] Fan L, Wang J, Xu Z, Yang X. (2022) A Reverse Modeling Method Based on CAD Model Prior and Surface Modeling. Machines, 10(10):905.

[27] Rojas-Sola JI, Río-Cidoncha G Del, Ortíz-Marín R, Trenas-Arbizu J. (2021) An Approach to the Study of a 19th-Century Sugarcane Mill and Steam Engine through CAD Techniques and Mechanical Engineering. Machines, 9(11):295.

[28] Toledano-García AA, Pérez-Cabrera HR, Ortega-Cabrera D, Navarro-Durán D, Pérez-Hernández EM. (2023) Trajectory Generator System for a UR5 Collaborative Robot in 2D and 3D Surfaces. Machines, 11(9):916.

[29] Bhandari B, Manandhar P. (2023) Integrating Computer Vision and CAD for Precise Dimension Extraction and 3D Solid Model Regeneration for Enhanced Quality Assurance. Machines, 11(12):1083.

[30] Huaizhong Li, Le MD, Gong ZM, Lin W. (2009) Motion Profile Design to Reduce Residual Vibration of High-Speed Positioning Stages. IEEE/ASME Trans Mechatronics, 14(2):264–269.

[31] Ha C-W, Rew K-H, Kim K-S. (2013) Robust Zero Placement for Motion Control of Lightly Damped Systems. IEEE Trans Ind Electron, 60(9):3857–3864.

[32] Ha C-W, Lee D. (2018) Analysis of Embedded Prefilters in Motion Profiles. IEEE Trans Ind Electron, 65(2):1481–1489.

[33] Bai Y, Chen X, Sun H, Yang Z. (2018) Time-Optimal Freeform S-Curve Profile Under Positioning Error and Robustness Constraints. IEEE/ASME Trans Mechatronics, 23(4):1993–2003.

[34] (2003) Lift (Elevators)–Measurement of Lift Ride Quality.